6. T.W. Eubanks and K. Chang, A compact parallel-plane perpendicular-current feed for a modified equiangular spiral antenna, IEEE Trans Antennas Propag 58 (2010), 2193–2202.
7. M.Y. Li, K. Tilley, J. McCleary, and K. Chang, Broadband coplanar waveguide-coplanar strip-fed spiral antenna, Electron Lett 31 (1995), 4–5.
8. P.C. Werntz and W.L. Stutzmann, Design, analysis and construction of an Archimedean spiral antenna and feed structure, Proc IEEE 1 (1989), 308–313.
9. N. Liu, P. Yang, and W. Wang, Design of a miniaturized ultra-wideband compound spiral antenna, IEEE International Conference on Microwave Technology & Computational Electromagnetics (ICMTCE), 2013, 255–258.
10. H. Wheeler, Transmission-line properties of parallel strips separated by a dielectric sheet, IEEE Trans Microwave Theory Tech 13 (1965), 172–185.
11. S.G. Kim and K. Chang, Ultrawide-band transitions and new microwave components using double-sided parallel-strip lines, IEEE Trans Microwave Theory Tech 52 (2004), 2148–2152.
12. J.-X. Chen, Double-sided parallel-strip line circuit analysis and applications to microwave component designs, Ph.D. thesis, City University of Hong Kong, 2008

RESONANCES OF ELECTROMAGNETIC OSCILLATIONS IN A SPHERICAL METAL NANOPARTICLE

B.A. Belyaev[1,2,3] and V.V. Tyurnev[1,2]
[1] Kirensky Institute of Physics, Siberian Branch, Russian Academy of Sciences, Krasnoyarsk, Russia; Corresponding author: belyaev@iph.krasn.ru
[2] Institute of Engineering Physics and Radio Electronics, Siberian Federal University, Krasnoyarsk, Russia
[3] Reshetnev Siberian State Aerospace University, Krasnoyarsk, Russia

Received 24 December 2015

ABSTRACT: *Electrodynamic analysis of plasma oscillations in a spherical metal nanoparticle is performed. It is shown that typical reduction in the frequency and quality factor of the resonances with increasing nanoparticle radius fades if the mode number grows. Depending on the particle radius, the resonant enhancement of the electric field might considerably either increase or decrease with increasing mode number.* © 2016 Wiley Periodicals, Inc. Microwave Opt Technol Lett 58:1883–1886, 2016; View this article online at wileyonlinelibrary.com. DOI 10.1002/mop.29930

Key words: *plasmonics; scattering; particles; resonators; resonant modes*

1. INTRODUCTION

It is well known that metal nanoparticles exhibit resonant properties under the impact of electromagnetic fields in the optical frequency range [1–3]. This phenomenon was discovered and explained as long ago as the beginning of the last century [4,5]. However, it is only in recent years the number of theoretical and experimental works on the optical properties of the metal nanoparticles begins to increase because of the development of nanotechnologies, and above all, the appearance of new problems in photonics and nanoelectronics. Resonances in metal nanoparticles are related to the oscillations of conduction electrons [6]. Their frequencies are considerably lower than the plasma frequency, ω^{p}, in continuous medium. Besides, the unloaded quality factor is sufficiently large for application. We note that the resonances occur due to both the skin depth in metals at optical frequencies and electron mean free path are much greater than the sizes of the articles.

Metal nanoparticles are widely used in biomedicine [7] and various biosensors are built using these [8]. These nanoparticles are also used for enhancing the effect of Raman scattering [9] and for the enhancement of fluorescence [10]. The possibility of applying these nanoparticles to the building of microwaveguides for the optical band is currently being investigated [11,12]. These microwaveguides represent chains of identical interacting nanoparticles, which can be considered as resonators, such that the chains have transparency windows for electromagnetic oscillations in the range of the resonant frequencies. We note that the wavelength of the propagating electromagnetic waves in the microwaveguides is much greater than the cross-sectional size of the nanoparticles of which they are formed. It is important to note also that analogous approaches are used in the design of waveguides based on interacting oscillating circuits [13] and microstrip resonators [14], which showed themselves to good advantage in the high and super-high frequency ranges.

In essence, such waveguides are passband filters of a high order whose bandwidth is proportional to the interaction of the resonators [15]. The interaction strength is determined first by the spacing between the resonators and their quality factor. However, in a chain of interacting resonators, including a chain of spherical nanoparticles, forming a waveguide, the coupling between the structural elements may weaken considerably if the resonant frequencies of these elements are mismatched. Therefore, it is important to study the regularities of the size-dependent behavior of the key resonance characteristics of the spherical metal nanoparticles when they are in a high-frequency electric field.

In this letter, we study the behavior of resonant frequencies, the quality factors of the resonances, near-field patterns, the enhancement coefficients of the electric field, and the frequency dependences of the scattering cross-sections of electromagnetic waves. We investigate three lower oscillation modes, taking into account the fact that the spherical resonators may efficiently interact not only at the frequency of the first oscillation mode but also at the frequencies of higher modes.

2. INITIAL FORMULAS

Let a spherical metal nanoparticle of radius r_0 be situated in a medium with relative permittivity ε_2 (Fig. 1). The dielectric properties of the nanoparticle material are described using the complex permittivity, $\varepsilon_1(\omega)$, that takes into account both dielectric and ohmic loss.

We shall consider the oscillations in the nanoparticle under the impact of an incident plane wave, with the following components of the electric and magnetic field

$$\begin{aligned} E_x(z,t) &= E_0 \exp\left(ik_2 z - i\omega t\right), \\ H_y(z,t) &= H_0 \exp\left(ik_2 z - i\omega t\right), \end{aligned} \tag{1}$$

where $k_2=\omega\sqrt{\varepsilon_0\varepsilon_2\mu_0}$, $H_0=E_0/Z_2$, $Z_2=\sqrt{\mu_0/(\varepsilon_0\varepsilon_2)}$, and ε_0 and μ_0 are the absolute permittivity and permeability of free space, respectively.

Using the general solution to this electrodynamic problem [16], we write the amplitudes of the nonzero components of the electric field of the scattered wave using a spherical coordinate system, for the convenience of further analysis, in the following form

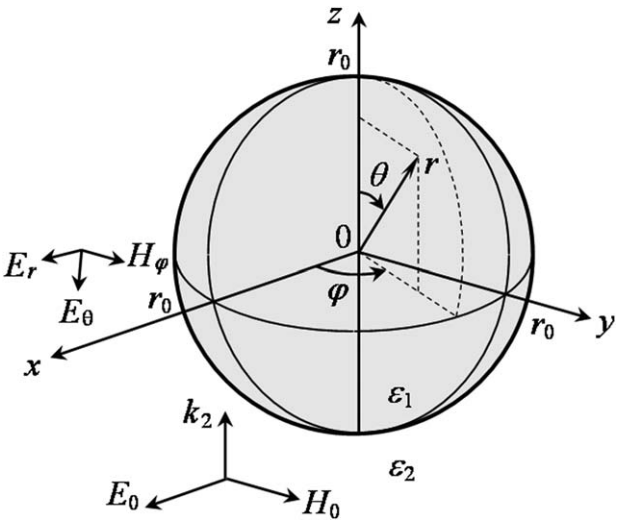

Figure 1 Metal nanoparticle of radius r_0 under the field of the electromagnetic wave

$$E_r^{sc}=E_0\sum_{n=1}^{\infty}i^{n+1}\frac{2n+1}{n(n+1)}\left[\frac{n(n+1)}{k_2r}h_n^{(1)}(k_2r)P_n^1(\cos\theta)A_n^e\right]\cos\varphi,$$

$$E_\theta^{sc}=E_0\sum_{n=1}^{\infty}i^{n+1}\frac{2n+1}{n(n+1)}\left[\begin{array}{l}\dfrac{[k_2r\cdot h_n^{(1)}(k_2r)]'}{k_2r}\dfrac{dP_n^1(\cos\theta)}{d\theta}A_n^e\\ \\ +ih_n^{(1)}(k_2r)\dfrac{P_n^1(\cos\theta)}{\sin\theta}A_n^m\end{array}\right]\cos\varphi,$$

$$E_\varphi^{sc}=E_0\sum_{n=1}^{\infty}i^{n+1}\frac{2n+1}{n(n+1)}\left[\begin{array}{l}-\dfrac{[k_2r\cdot h_n^{(1)}(k_2r)]'}{k_2r}\dfrac{P_n^1(\cos\theta)}{\sin\theta}A_n^e\\ \\ -ih_n^{(1)}(k_2r)\dfrac{dP_n^1(\cos\theta)}{d\theta}A_n^m\end{array}\right]\sin\varphi, \quad (2)$$

where A_n^e and A_n^m are expansion coefficients that are the amplitudes of the electrical (e) and magnetic (m) multipole oscillations of the nth order that have a longitudinal component of either the electric or magnetic field, respectively. A prime symbol above a bracket refers to the differentiation with respect to k_2r, and $h_n^{(1)}(k_2r)$ is a spherical Bessel function of the third kind, $P_n^1(\cos\theta)$ is the associated Legendre function of the first kind, of the first order and nth power. The amplitudes A_n^e and A_n^m are expressed by the following formulas

$$A_n^e=\frac{j_n(\theta_2)[\theta_1j_n(\theta_1)]'-\frac{\varepsilon_1}{\varepsilon_2}j_n(\theta_1)[\theta_2j_n(\theta_2)]'}{h_n^{(1)}(\theta_2)[\theta_1j_n(\theta_1)]'-\frac{\varepsilon_1}{\varepsilon_2}j_n(\theta_1)[\theta_2h_n^{(1)}(\theta_2)]'},$$

$$A_n^m=\frac{j_n(\theta_2)[\theta_1j_n(\theta_1)]'-\frac{\varepsilon_1}{\varepsilon_2}j_n(\theta_1)[\theta_2j_n(\theta_2)]'}{j_n(\theta_2)[\theta_1j_n(\theta_1)]'-\frac{\varepsilon_1}{\varepsilon_2}h_n^{(1)}[\theta_2h_n^{(1)}(\theta_2)]'}, \quad (3)$$

where $\theta_1=k_1r_0$, $\theta_2=k_2r_0$, $k_i=\omega\sqrt{\varepsilon_0\varepsilon_i\mu_0}$. We shall compute the complex permittivity of the nanoparticle using the formula

$$\varepsilon_1(\omega)=1-\frac{\omega_p^2}{\omega^2+i\omega\gamma} \quad (4)$$

in accordance with the Drude model [6]. Here $\omega_p=e\sqrt{N/(m^*\varepsilon_0)}$ is the plasma frequency, e is the absolute value of the electron charge, N is the electron density, m^* is the effective electron mass, σ_0 is DC conductivity, and $\gamma=Ne^2/(m^*\sigma_0)$ is the relaxation frequency of the charge carriers. For silver we obtain $\omega^p/(2\pi)=2171$ THz, $\gamma/(2\pi)=2.3$ THz if m^* is supposed to be equal to free-electron mass.

It is significant to note that in metal nanoparticles, the resonant frequencies of electrical oscillation modes (electrical multipoles) are lower than the frequencies of magnetic modes by several orders of magnitude. This is due to the manifestation of inertia of the conduction electrons only in electrical oscillation modes. Our computation shows that it takes place the inequality $|A_n^e|\gg|A_n^m|$, therefore only electrical oscillation modes are excited efficiently in metal nanoparticles, whereas magnetic modes may be neglected.

It is clear that the roots, ω_n, of the equation

$$1/A_n^e(\omega)=0 \quad (5)$$

for each multipole excitation of the nanoparticle are the complex frequencies of the free plasma oscillations. Therefore, the resonant frequencies, f_n, and the loaded quality factors, Q_n, of the plasma oscillations may be computed using the formulas [17]

$$f_n=\mathrm{Re}\,(\omega_n)/(2\pi),\quad Q_n=-\mathrm{Re}\,(\omega_n)/(2\mathrm{Im}\,(\omega_n)). \quad (6)$$

3. RESULTS OF ELECTRODYNAMIC ANALYSIS

Figure 2 shows the dependences of the resonant frequencies and the quality factors on the radius of the metal nanoparticle for first three modes of the plasma oscillations, and for two

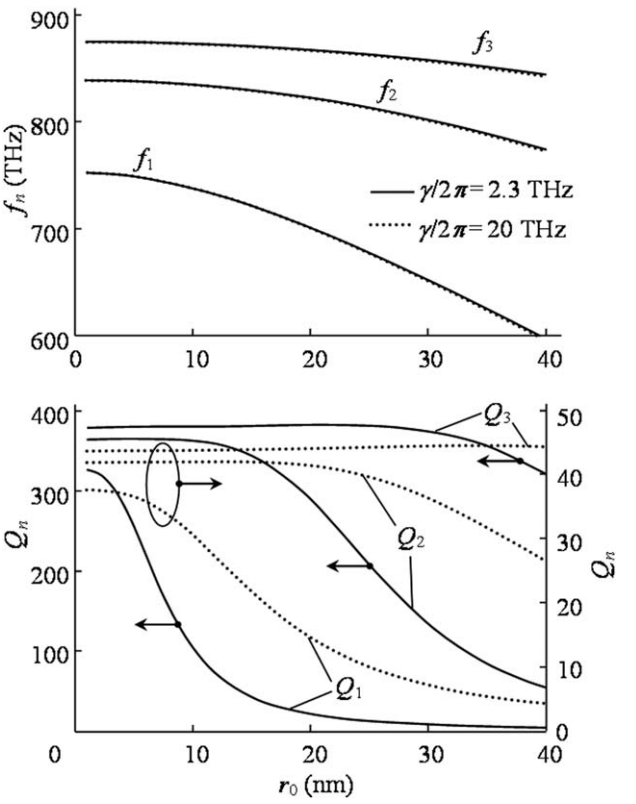

Figure 2 Dependences of the resonant frequencies and loaded quality factors of the nanoparticle on radius, for two values of relaxation frequency

TABLE 1 Resonance Performances for Three First Oscillation Modes of Metal Nanoparticles with the Relaxation Frequency $\gamma/(2\pi)=2.3$ THz

r_0 (nm)	f_1 (THz)	f_2 (THz)	f_3 (THz)	Q_1	Q_2	Q_3	$\frac{E_1^{max}}{E_0}$	$\frac{E_2^{max}}{E_0}$	$\frac{E_3^{max}}{E_0}$
10	738	835	873	104	363	681	244	76	5.0
40	615	774	844	4.7	54	322	11.2	40.5	61.4

relaxation frequency values, γ. Note that γ determines the intrinsic quality factor of the plasma oscillations in the nanoparticle. The solid lines in Figure 2 correspond to the dependences for the value $\gamma/(2\pi)=2.3$ THz, which was estimated using the DC conductivity of bulk silver.

It is significant that the reduction of the quality factor of the resonances as the radius r_0 increases is due to an increase in the radiation loss of electromagnetic oscillations by the nanoparticle. We note also that the degree of the resonant frequency reduction with increasing particle size reduces monotonically with increasing oscillation mode number. Moreover, the dependences of the loaded quality factors on r_0 decay with increasing oscillation mode number, while the values themselves for the quality factors remain rather high. The obtained data indicates that the optical microwaveguides based on the chains of the electromagnetically coupled metal nanospheres will operate more efficiently when not the first oscillation mode [11,12], but the second or third mode is excited in the particles.

Indeed, in this case, the actual size-dispersion of the particles does not affect the attenuation per unit length in the microwaveguide because the resonant frequencies of these particles almost coincide. The high loaded quality factors of the resonators at the second and third oscillation modes indicate a low electromagnetic wave radiation loss into space of the particles. These high quality factors enable a high enhancement of the amplitude of the high-frequency electric field near the particle surface, as is shown below. This enables the particles to interact effectively with each other in the chain forming the microwaveguide.

Table 1 shows the resonant frequencies, the loaded quality factors, and the enhancement coefficients of the external electric field; all the figures are given for the three oscillation modes in the particles of two sizes. A relaxation frequency $\gamma/(2\pi)=2.3$ THz was used in our computation. It is seen that the frequencies of the first resonance for particle radiuses of 10 and 40 nm differ by almost 20%, while the frequencies of the second and third resonances differ only by 7% and 3%, respectively. For the same radius values, the quality factors of the first oscillation mode differ by over 20 times, the quality factors of the second oscillation mode differ by almost seven times, and the quality factors of the third oscillation mode differ by approximately two times. It is of interest that the enhancement coefficients of the external electric field (E_n/E_n^{max}) for the smaller particle ($r_0 = 10$ nm) decrease with increasing oscillation mode number, while for the larger particle ($r_0 = 40$ nm) these coefficients increase. It is clear that this established fact should be taken into account when choosing the nanoparticle sizes while designing a microwaveguide.

Figure 3 shows the near-field pattern of the radial components of the electric fields that were computed for the first three oscillation modes of the nanoparticle near its surface, where every radial component is normalized to its maximum value (E_n/E_n^{max}). As expected, the normalized near-field pattern does not depend on the nanoparticle size, which is in contrast with the resonance behaviors.

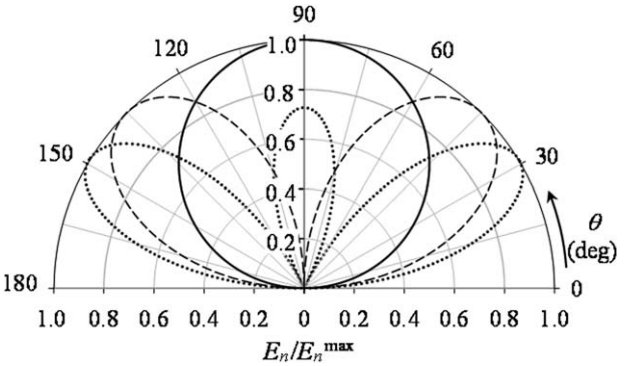

Figure 3 Normalized near-field pattern of the high-frequency electric field at the resonant frequencies of the first (*solid line*), second (*dashed line*), and third (*dotted line*) oscillation modes of the metal nanoparticle

The important characteristics of a particle that is placed in any medium are its cross-sections of scattering and the absorption of electromagnetic waves, together with their sum – the extinction cross-section. We note that loss of power, transmitted through the medium with the particles, is proportional to the extinction cross-section. When the electrical multipole of the nth order is excited in the spherical particle, the scattering cross-section, $\sigma_{sc}{}^n$, and the extinction cross-section, $\sigma_{ex}{}^n$, normalized to the area of the particle cross-section, πr_0^2, are related with the amplitudes A_n^e by the known formulas [16]

$$\sigma_{sc}^n = 2\frac{2n+1}{\theta_2^2}|A_n^e|^2, \qquad \sigma_{ex}^n = 2\frac{2n+1}{\theta_2^2}\mathrm{Re}\,A_n^e. \tag{7}$$

It is clear that the total scattering cross-section, σ_{sc}, and the total extinction cross-section, σ_{ex}, of the particle are the sum of $\sigma_{sc}{}^n$ and the sum of $\sigma_{ex}{}^n$ over all values of n, respectively.

For the case of the silver nanoparticle surrounded by water, Figure 4 shows the computed dependence of the normalized extinction cross-section on the wavelength, λ. The computation was carried out for the relative permittivity of the surrounding medium, $\varepsilon_2 = 1.76$, the plasma frequency, $\omega^p/(2\pi)=1600$ THz, and the relaxation frequency, $\gamma/(2\pi)=20$ THz.

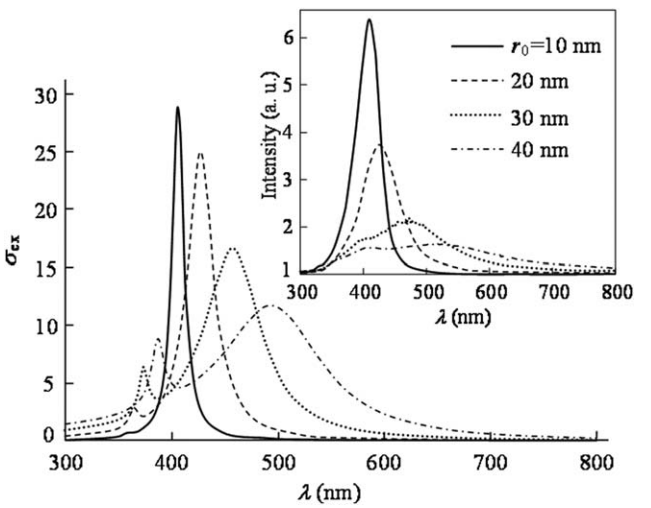

Figure 4 Dependences of the normalized extinction cross-section on the wavelength, computed for various particle radiuses. The inset shows the measured dependences of the extinction of light in colloidal solutions of silver in water [18]

In the inset of this figure, the experimental results that were obtained in [18] are given for comparison. In the experiment, the value of the light extinction for the four samples of water colloidal solutions of silver nanoparticles that differed in size was measured. In the computation we reduced ω^{p} by approximately a quarter and increased γ by more than eight times relative to the frequencies computed for m^* that was supposed to be equal to free-electron mass. That was done in order to bring the resonances of $\sigma_{\mathrm{ex}}(\lambda)$ closer to the observed resonances in the experiment and to get the reasonable proportion between the amplitudes of the resonances. Besides the fundamental resonances in the experimental curves in Figure 4, one can observe the resonances corresponding to the second oscillation modes at shorter wavelengths. These resonances are especially apparent in the theoretical results.

4. CONCLUSION

Thus, the conducted electrodynamic analysis of the plasma oscillations in a spherical metal nanoparticle placed into an infinite dielectric medium enabled the examination of the dependences of the resonant frequencies and the resonance quality factors on the radius of the particle. Through evaluation of the obtained results, we first showed that, with increasing nanoparticle radius, the typical lowering of the resonant frequency and the quality factor gradually vanishes with an increasing oscillation mode number. In addition, we showed that resonant enhancement of the electric field near the particle surface might both significantly increase and decrease as the particle radius increases depending on the oscillation mode number. These findings are of great importance to the design of optical microwave guides based on chains of coupled metal nanoparticles. A good agreement between the theoretical and experimental results proves the validity of the obtained electrodynamic analysis data for the resonant properties of the metal nanoparticles.

REFERENCES

1. K.L. Kelly, E. Coronado, L.L. Zhao, and G.C. Schatz, The optical properties of metal nanoparticles: The influence of size, shape, and dielectric environment, Phys Chem B 107 (2003), 668–677.
2. E.A. Coronado, E.R. Encina, and F.D. Stefani, Optical properties of metallic nanoparticles: Manipulating light, heat and forces at the nanoscale, Nanoscale 3 (2011), 4042–4059.
3. Q. Lin and Z. Sun, Study on optical properties of aggregated ultrasmall metal nanoparticles, Optik 122 (2011), 1031–1036.
4. R.W. Wood, On a remarkable case of uneven distribution of light in a diffraction grating spectrum, Philos Mag Ser 6 4 (1902), 396–402.
5. G. Mie, Beiträge zur Optik trüber Medien, speziell kolloidaler Metallösungen, Ann Phys 25 (1908), 377–445.
6. P. Drude, Zur Elektronentheorie der Metalle, Ann Phys 306 (1900), 566–613.
7. V.V. Mody, R. Siwale, A. Singh, and H.R. Mody, Introduction to metallic nanoparticles, J Pharm Bioall Sci 2 (2010), 282–289.
8. A.A. Lazarides, K. Lance Kelly, T.R. Jensen, and G.C. Schatz, Optical properties of metal nanoparticles and nanoparticle aggregates important in biosensors, J Mol Struct (Theochem) 529 (2000), 59–63.
9. A. Wokaun, J.P. Gordon, and P.F. Liao, Radiation damping in surface-enhanced Raman scattering, Phys Rev Lett 48 (1982), 957–960.
10. J-S. Hong, Microstrip filters for RF/microwave applications, John Wiley & Sons, New York, 2011.
11. K.H. Fung, R.C.H. Tang, and C.T. Chan, Analytical properties of the plasmon decay profile in a periodic metal-nanoparticle chain, Opt Lett 36 (2011), 2206–2208.
12. R.S. Savelev, A.P. Slobozhanyuk, A.E. Miroshnichenko, Y.S. Kivshar, and P.A. Belov, Subwavelength waveguides composed of dielectric nanoparticles, Phys Rev B 89 (2014), 035435-1–035435-7.
13. R.R.A. Syms, I.R. Young, and L. Solymar, Low-loss magneto-inductive waveguides, J Phys D: Appl Phys 39 (2006), 3945–3951.
14. M.J. Freire, R. Marqués, M.A.G. Laso, and F. Medina, Planar magnetoinductive wave transducers: Theory and applications, Appl Phys Lett 85 (2004), 4439–4441.
15. B.A. Belyaev, A.A. Leksikov, and V.V. Tyurnev, Frequency-selective features of multisection filters based on regular microstrip resonators, J Commun Technol Electron 49 (2004), 1228–1236.
16. J.A. Stratton, Electromagnetic theory, McGraw-Hill, New York, 1941, Chapter IX.
17. B.A. Belyaev and V.V. Tyurnev, Analysis of the quality factor of the optical half-wavelength resonator, Microw Opt Technol Lett 55 (2013), 1613–1616.
18. W. Jacak, J. Krasnyj, J. Jacak, R. Gonczarek, A. Chepok, L. Jacak, D.Z. Hu, and D. Schaadt, Radius dependent shift in surface plasmon frequency in large metallic nanospheres: Theory and experiment, J Appl Phys 107 (2010), 124317-1–124317-13.

MIMO ANTENNA WITH HIGH FREQUENCY SELECTIVITY AND CONTROLLABLE BANDWIDTH FOR BAND-NOTCHED UWB APPLICATIONS

Hui-Fen Huang and Shu-Guang Xiao
School of Electronic and Information Engineering, South China University of Technology, Guangzhou, 510641, China;
Corresponding author: huanghf@scut.edu.cn

Received 25 December 2015

ABSTRACT: *A multiple-input–multiple-output (MIMO) antenna with high frequency selectivity and controllable bandwidth, is proposed for band-notched ultrawideband (UWB) applications. In other words, it has a bandstop-filter-like response (second-order notched band) at the aimed rejected band. It consists of two rectangular printed monopole (PM) elements and a simple stepped ground stub to enhance wideband isolation. For achieving the second-order rejected band of the IEEE 802.11 wireless local area network (WLAN) band from 5.15 to 5.85 GHz centered at 5.5 GHz, two parasitic modified split-ring resonators (PMSRRs) and two inverted L-shaped branches (ILBs), are utilized. Measured results prove a bandwidth of $S_{11} < -10$ dB and $S_{12} < -15$ dB at 2.8–12 GHz excluding a rejection band of 5–5.95 GHz. Its size is only 32 × 26 mm^2 on a cost-effective FR4 substrate.* © 2016 Wiley Periodicals, Inc.
Microwave Opt Technol Lett 58:1886–1891, 2016; View this article online at wileyonlinelibrary.com. DOI 10.1002/mop.29929

Key words: *antenna; multiple-input–multiple-output; frequency selectivity; controllable bandwidth; band-notched; wireless local area network; ultrawideband (UWB)*

1. INTRODUCTION

Multiple-input–multiple-output (MIMO) technology [1] could augment channel capacity markedly without increasing frequency spectrum or input power. Ultrawideband (UWB) [2] is a new wireless communication technology having a high-speed data rate and large capacity. Hence, MIMO has been introduced to UWB antenna [3]. The UWB (3.1–10.6 GHz), overlaps with the IEEE 802.11 wireless local area network (WLAN) (5.15–5.85 GHz). Thus, one solution is to equip the antenna with band-notched characteristics [4–15].